Physicochem. Probl. Miner. Process., 54(2), 2018, 517-526

http://www.journalssystem.com/ppmp/

Physicochemical Problems of Mineral Processing

ISSN 1643-1049

Received July 13, 2017; reviewed; accepted November 8, 2017

Study on recovery of lead, zinc, iron from jarosite residues and simultaneous sulfur fixation by direct reduction

Yayun Wang, Huifen Yang, Weihao Zhang, Ronglong Song, Bo Jiang

School of Civil and Resource Engineering, University of Science and Technology Beijing, 30 Xueyuan Road, Haidian District, Beijing, 100083 China

Corresponding author: yanghf@ustb.edu.cn (Huifen Yang), wangyy128@hotmail.com (Yayun Wang)

Abstract: Jarosite residues, which are generated in a zinc production plant by a hydrometallurgical process, contain a large amount of valuable metal components. In this study, a method was proposed for the recovery of lead, zinc and iron from the residues and simultaneous sulfur fixation through direct reduction followed by magnetic separation. The influences of the roasting temperature, roasting time and the concentration of SO_2 gas in the direct reduction process were researched in detail. Results showed that the volatilization rates of lead, zinc and sulfur were 96.97%, 99.89% and 1.09%, respectively, and the iron metallization rate was 91.97% under optimal reduction conditions; roasting temperature 1523 K for 60 min. The magnetic concentrate with the iron content of 90.59% and recovery rate of 50.87% was obtained from the optimal reduction product by grinding and magnetic separation. The optimum fineness for separation 96.56% less than 37 μm accounted with magnetic field strength 24 kA/m. The theoretical analysis was carried out by thermodynamics, X-ray powder diffraction, gas analysis and scanning electron microscopy.

Keywords: *jarosite, direct reduction, recovery, valuable metal, sulfur fixation*

1. Introduction

Currently, about 75% of the world's zinc metal is produced by hydrometallurgical methods through acid leaching (Montanaro et al., 2001; Calla-Choque et al., 2016). During the zinc extraction process, jarosite residues are produced when eliminating iron from leaching solutions (Pappu et al., 2006; Kerolli-Mustafa et al., 2016). According to estimations, more than one million tons of this kind of residue was stored up in China per year (Ju et al., 2011). This jarosite can cause serious harm to environment and human health as it contains some toxic elements, such as As, Cd, Pb, Zn and S (Özverdi and Erdem, 2010; Erdem and Özverdi, 2011). Therefore, developing methods to convert jarosite into non-hazardous form is an urgent task.

Many studies on the utilization of jarosite residues have been carried out, which have mainly concentrated on the utilization of jarosite as construction material (Asokan et al., 2010; Asokan et al., 2006) and recovery of contained non-ferrous metals such as Pb, Zn, Cd, Ag, and Cu (Chen et al., 2009; Hu et al., 2014; Malenga et al., 2015). Asokan et al. (2006) presented an idea of overall utilization of jarosite residues as construction bricks. Jarosite, fly ash, clay and water were mixed in certain proportion for jarosite bricks production. However, the method did not recover the valuable metals. Haisheng Han et al. (2014) proposed a method of the recovery of anglesite ($PbSO_4$) and silver from jarosite residues by roasting combined with sulfidization-flotation. The jarosite was first roasted at 873-973 K and then processed by flotation to recover lead and silver. However, it did not take into account the evaporation of SO_2 during the roasting process. Much of the research mainly focused on the recovery of non-ferrous metals from jarosite but ignore the recovery of iron.

On the other hand, considerable research has been done in iron recovery from solid wastes through direct reduction followed by magnetic separation (Guo et al., 2015; Sun et al., 2015; Yu et al., 2015).

http://dx.doi.org/10.5277/ppmp1859

Iron can be recovered effectively from vanadium tailing (Yang et al., 2011), red mud (Liu et al., 2009), oily hot rolling mill sludge (Park et al., 2002) and copper matte smelting slag (Maweja et al., 2009) with a direct reduction-magnetic separation technique. Lead and zinc can also be recovered effectively from zinc leaching residues by direct reduction (Gang et al., 2015).

Based on the above research, a new method is presented in this study for the comprehensive recovery of lead, zinc, iron from jarosite residues and simultaneous sulfur fixation by direct reduction. The key features of this work are that the valuable components lead, zinc, iron can be recovered from jarosite and the hazardous element sulfur can be fixed in the roasting product.

2. Experimental

2.1 Materials

The jarosite residues sample used in this work was obtained from Shaanxi province, China. Its chemical composition is shown in Table 1. The X-ray powder diffraction (XRD) analysis of jarosite residues sample found that the main phases were $NH_4Fe_3(SO_4)_2(OH)_6$, $Pb(Fe_3(SO_4)_2(OH)_6)_2$ and $ZnFe_2O_4$, as shown in Fig. 1.

The coal used in this study is bituminous coal. Its industrial analysis (air dry) is listed in Table 2. In order to promote the sulfur fixation in the roasting product rather than volatilization into air, analytical grade CaO is added.

Table 1. Chemical composition of jarosite residues

Constituent	Fe	Zn	Pb	S	Al_2O_3	As	SiO_2	MgO	CaO
Content (wt-%)	26.76	6.95	3.01	10.16	1.78	0.33	4.74	0.50	1.83

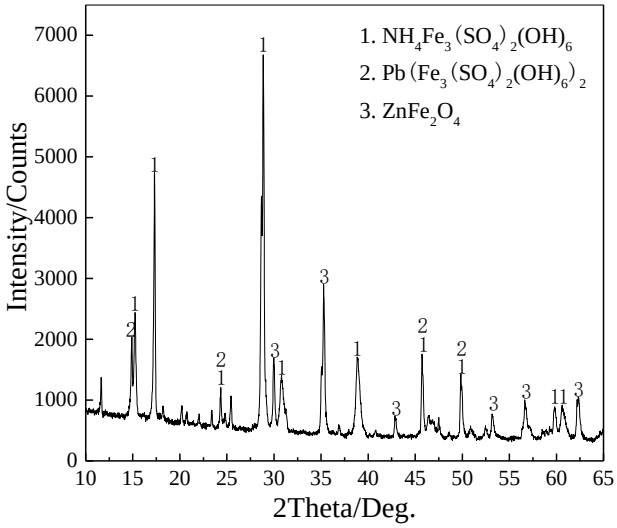

Fig. 1. XRD patterns of jarosite residues

Table 2. Industrial analysis of bituminous coal

Constituent	Moisture	Ash	Volatiles	Fixed carbon	Sulfur
Content (wt-%)	4.56	17.36	28.88	49.20	0.13

2.2 Experimental methods

The study was mainly divided in two sections: The direct reduction roasting and the milling-magnetic separation. The schematic diagram of full process flow is shown in Fig. 2. The chief feature of this process is the stepwise recovery of valuable metals from jarosite, harmful element sulfur is fixed in the reduction product at the same time. The lead and zinc that were volatilized in gaseous form could be collected by specialized dust collection equipment. In practical production, the lead and zinc were

returned to the zinc hydrometallurgical process in the original factory to recycle lead and zinc. The tailings containing large amounts of CaS could be used as a S^{2-} precipitant for treating heavy metal ions from wastewater in the factory.

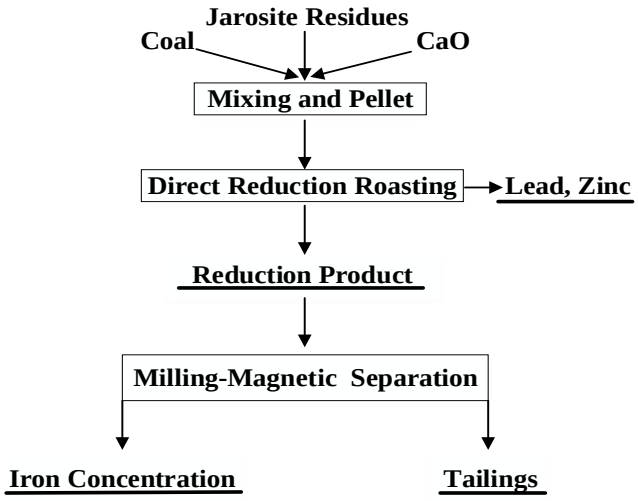

Fig. 2. Schematic diagram of full process flow

2.2.1 Direct reduction roasting

Jarosite, CaO, coal and water were fully-mixed together according to mass ratio of coal, CaO and water to jarosite of 25:27.5:35:100, and then the mixture was pressed to pellets. The crucible containing pellets was put into the furnace and held for scheduled time at the selected temperature. The SO_2 gas concentration was monitored during the roasting process. Afterwards, the roasting pellets were cooled to room temperature. Then the lead, zinc, sulfur, total iron and metallic iron content in roasting pellets were analyzed by chemical method.

The recovery of lead and zinc in this study is represented by volatilization rate of lead and zinc. The volatilization rates of lead, zinc and sulfur were calculated according to equation

$$\mathrm{V} = 1 - \frac{C_2 \times W_2}{C_1 \times W_1} \times 100\% \tag{1}$$

and the iron metallization rate was calculated by equation

$$\mathrm{M} = \frac{C_M}{C_T} \times 100\% \tag{2}$$

where V is the volatilization rate of lead, zinc or sulfur, C_1 and C_2 are the concentration of lead, zinc or sulfur in jarosite and reduction product respectively, W_1 and W_2 are the weight of the jarosite and reduction product respectively, M is the iron metallization rate, C_M is the concentration of metallic iron in the reduction product, C_T is the concentration of total iron in the reduction product.

2.2.2 Recovery of iron by milling-magnetic separation

The reduction product was crushed to -2 mm and then ground using wet grinding. The XCGS-73 low intensity magnetic separator with a magnetic field intensity of 24 kA/m was used to recover metallic iron from roasting product. The total iron content in magnetic concentrate was analyzed by chemical method.

2.3 Reaction mechanisms

Fig. 3 shows the differential thermal patterns of jarosite from 298 K to 1473 K, which showed that the jarosite residues went through four stages in this roasting process. In the first stage (298-393 K), jarosite residues lost free and absorbed water. The second stage (393-653 K) was a crystallization water removing process of jarosite. In the third stage (653-743 K), an exothermic decomposition peak was

outstanding, and jarosite started to decompose into mikasaite ($Fe_2(SO_4)_3$), and ammonia (NH_3). In the last stage (743-1473 K), mikasaite ($Fe_2(SO_4)_3$) was decomposed into hematite (Fe_2O_3) and sulfur dioxide (SO_2) (Frost et al., 2006; Han et al., 2014).

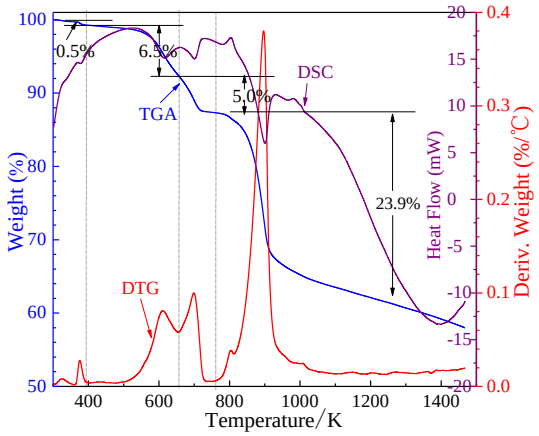

Fig. 3. Differential thermal patterns of jarosite (TGA: thermos gravimetric analysis; DSC: differential scanning calorimetry; DTG: derivative thermogravimetry)

$NH_4Fe_3(SO_4)_2(OH)_6$ and $Pb(Fe_3(SO_4)_2(OH)_6)_2$ were decomposed into NH_3, $Fe_2(SO_4)_3$, $PbSO_4$, SO_2, etc. about at 673 K. The reaction mechanisms can be expressed with the following equations (3) - (11) (Gang et al., 2015; Guo et al., 2015; Liu et al., 2015; Yang et al., 2011):

$$Fe_2(SO_4)_3 + 4C = 2FeO + 3SO_2(g) + 4CO(g) \quad \triangle G^{\theta}=699.52 - 1.29T\ (kJ/mol) \quad (3)$$

$$ZnFe_2O_4 + 2C = Zn(g) + 2FeO + 2CO(g) \quad \triangle G^{\theta}=546.19 - 0.49T\ (kJ/mol) \quad (4)$$

$$PbSO_4 + 2C = Pb(g) + SO_2(g) + 2CO(g) \quad \triangle G^{\theta}=577.13 - 0.62T(kJ/mol) \quad (5)$$

$$Fe_2(SO_4)_3+4CO(g) = 2FeO+3SO_2(g)+4CO_2(g) \quad \triangle G^{\theta}=12.85 - 0.58T\ (kJ/mol) \quad (6)$$

$$ZnFe_2O_4+ 2CO(g) = Zn(g) + 2FeO + 2CO_2(g) \quad \triangle G^{\theta}=202.85 - 0.14T(kJ/mol) \quad (7)$$

$$PbSO_4 + 2CO(g) = Pb(g) + SO_2(g) + 2CO_2(g) \quad \triangle G^{\theta}=233.79 - 0.27T(kJ/mol) \quad (8)$$

$$2FeO + C = 2Fe + CO_2(g) \quad \triangle G^{\theta}=135.78 - 0.13T\ (kJ/mol) \quad (9)$$

$$CaO + 1.5C + SO_2(g) = CaS + 1.5CO_2(g) \quad \triangle G^{\theta}=-132.09 - 0.08T\ (kJ/mol) \quad (10$$

$$CaO + 3CO(g) + SO_2(g) = CaS + 3CO_2(g) \quad \triangle G^{\theta}=-389.59 - 0.18T(kJ/mol) \quad (11)$$

2.4 Analysis and characterization

The chemical analyses of jarosite and reduction product were conducted by China University of Geosciences (Beijing) analysis laboratory. The mineral and compositions of jarosite, reduction product and magnetic tailings were investigated by X-ray powder diffraction method (XRD) using Cu-K radiation at the scanning rate of 10 °/min from 10° to 90°. The differential thermal patterns of jarosite were analyzed by Peking University analysis laboratory (Dupont 1090B). The SO_2 gas concentration was detected by Germany MRU VARIO PLUS enhanced gas analyzer. The microstructures of above products were also analyzed by scanning electron microscope (SEM) with energy dispersive spectrum (EDS) (Carl Zeiss EVO18), the sample for analysis was mounted in epoxy resin and polished.

3. Results and discussion

3.1 Procedure of direct reduction

To optimize roasting temperature, various temperatures were studied while keeping roasting time of 120 min. The effect of roasting temperature on direct reduction is shown in Fig. 4.

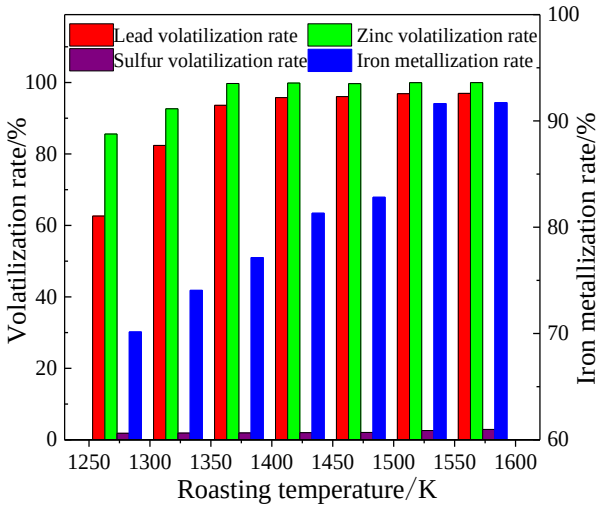

Fig. 4. Effect of roasting temperature on direct reduction

Fig. 4 showed that the roasting temperature had considerable influence on the lead, zinc volatilization rates and iron metallization rate. When roasting temperature increased from 1273 K to 1423 K, the volatilization rates of lead and zinc increased from 62.62% to 95.77% and from 85.59% to 99.85%, respectively. However, further increase in the roasting temperature did not cause an increase in the volatilization rates of lead and zinc. The roasting temperature was conducive to the iron metallization rate. The iron metallization rate increased sharply especially when roasting temperature increased from 1273 K to 1523 K, and then kept stable. The roasting temperature had little effect on the volatilization of sulfur, which basically was constant with increasing roasting temperature but remained less than 3% from 1273 K to 1573 K. Considering the results above, the optimal roasting temperature was selected as 1523 K.

The XRD patterns of reduction product at different roasting temperatures were determined to find out temperature effect mechanism on direct reduction. The XRD results are shown in Fig. 5.

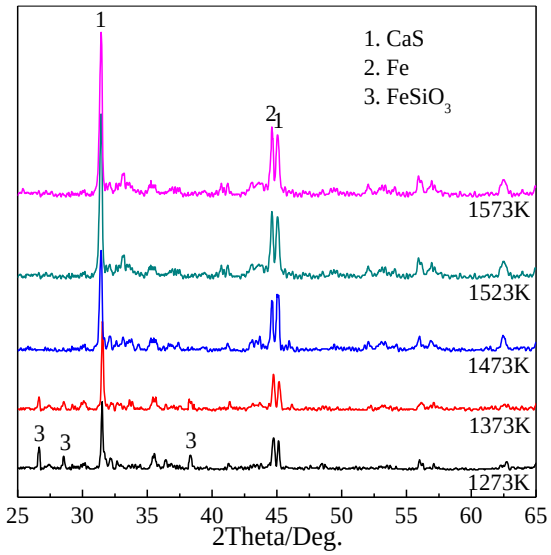

Fig. 5. XRD patterns of reduction product at different roasting temperatures

Fig. 5 showed that CaS, metallic iron and some $FeSiO_3$ were main phases of reduction product. The feasibility of the $FeSiO_3$ existence and the transforming $FeSiO_3$ into metallic iron is shown in equations (12) and (13)

$$FeO + SiO_2 = FeSiO_3 \qquad \triangle G^{\theta}=-17.54+0.006T\ (kJ/mol) \qquad (12)$$

$$2FeSiO_3 + C = 2Fe + 2SiO_2 + CO_2(g) \qquad \triangle G^{\theta}=170.87-0.15T\ (kJ/mol) \qquad (13)$$

Within the temperature range from 273 K to 1573 K, the free energy ($\triangle G^{\theta}$) of reaction (12) is below zero. Thus, $FeSiO_3$ could exist in roasting process. The free energy ($\triangle G^{\theta}$) of reaction (13) is positive zero at 1173 K and less than zero at 1273 K. Therefore, $FeSiO_3$ could be reduced to metallic iron above 1273 K, and the reduction effect is more obvious with the increase of roasting temperature. According to Fig. 5, the $FeSiO_3$ diffraction peaks existed at 1273 K, which gradually weakened with the increase of roasting temperature and disappeared when the roasting temperature was over 1473 K. With the increase of roasting temperature, the diffraction peaks of metallic iron increased little by little, and remained constant when the temperature exceeded 1523 K. In Fig. 5, CaS was one of the main phases meaning that sulfur was fixed in the roasting product in the form of CaS.

The different roasting times were researched at constant temperature 1523 K. The effect of roasting time on direct reduction is shown in Fig. 6.

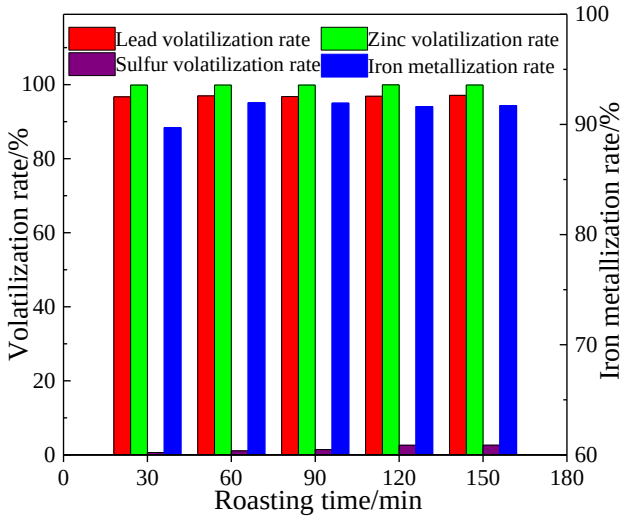

Fig. 6. Effect of roasting time on direct reduction

Fig. 6 showed that within the roasting time range from 30 min to 150 min, roasting time had insignificant effect on the volatilization rates of lead and zinc. At this time range, the volatilization rates of lead and zinc were greater than 96.5% and 99.8%, respectively. The iron metallization rate increased from 89.7% at 30 min to 91.9% at 60 min, but then maintained constant at longer times. The sulfur volatilization rate marginally increased with the increase of roasting time from 30 min to 150 min, but remained less than 2.7% within this tested range. The optimal roasting time was determined for 60 min.

In summary, the optimal roasting temperature was 1523 K and the roasting time was 60 min. Under these conditions, the volatilization rates of lead, zinc and sulfur were 96.97%, 99.89% and 1.09% respectively, the iron metallization rate was 91.97%.

3.2 SO_2 gas analysis

In order to study the difference of released SO_2 gas in jarosite and mixed pellets during the roasting process, the SO_2 gas concentration was measured, as shown in Fig. 7. As shown in Fig. 7, the SO_2 gas concentrations of the jarosite and the pellets were significantly different during the roasting process. At the initial stage of roasting, SO_2 gas concentration of jarosite was almost zero, increased rapidly when the roasting time was over 40 min and reached the maximum at about the 82 min. Afterwards, the SO_2 gas concentration dropped drastically from 82 min to 140 min and then nearly kept constant after 140 min. The SO_2 gas concentration of pellets was far less than that of jarosite, it achieved a minor peak at about 100 min and then reduced at longer roasting time. This is because SO_2 was volatilized directly in the jarosite roasting process. Nevertheless, the pellets, containing CaO and coal, can fix sulfur in the roasted production as shown in equations (10) and (11).

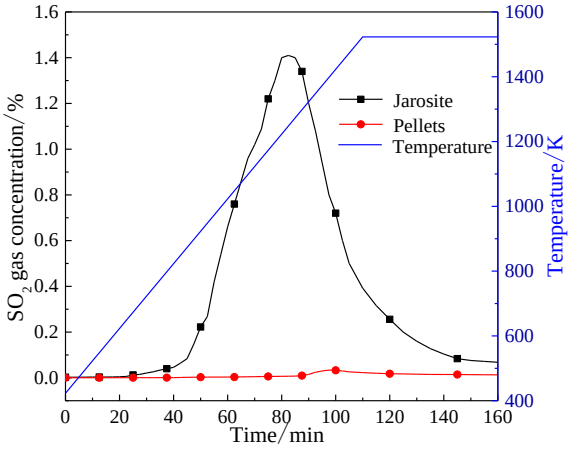

Fig. 7. SO_2 gas concentration of jarosite and mixed pellets in roasting process

3.3 Microstructure analysis

The jarosite sample and the reduction product under the optimum reduction conditions were analyzed by scanning electron microscope (SEM) coupled with energy dispersive spectroscopy (EDS), and the results are shown in Fig. 8. By comparing the SEM images of jarosite sample (Fig. 8 (a)) and reduction product under optimum conditions (Fig. 8 (b)), it was found that complicated jarosite was turned into several kinds of phases with clear boundaries in reduction product. The clear boundaries between iron particles and slag were easily seen (Fig. 8 (b)). Therefore, the separation of metallic iron particles could be achieved through grinding and their recovery by magnetic separation. As shown in Fig. 8 (c), (d), (e) and (f), the lead and zinc did not appear in the EDS, which indicated that lead and zinc had been volatilized into gaseous phase. Most of the sulfur in the reduction product was in the form of calcium sulfide and some sulfur was in the form of iron sulfide, as shown in Fig. 8 (d) and Fig. 8 (e).

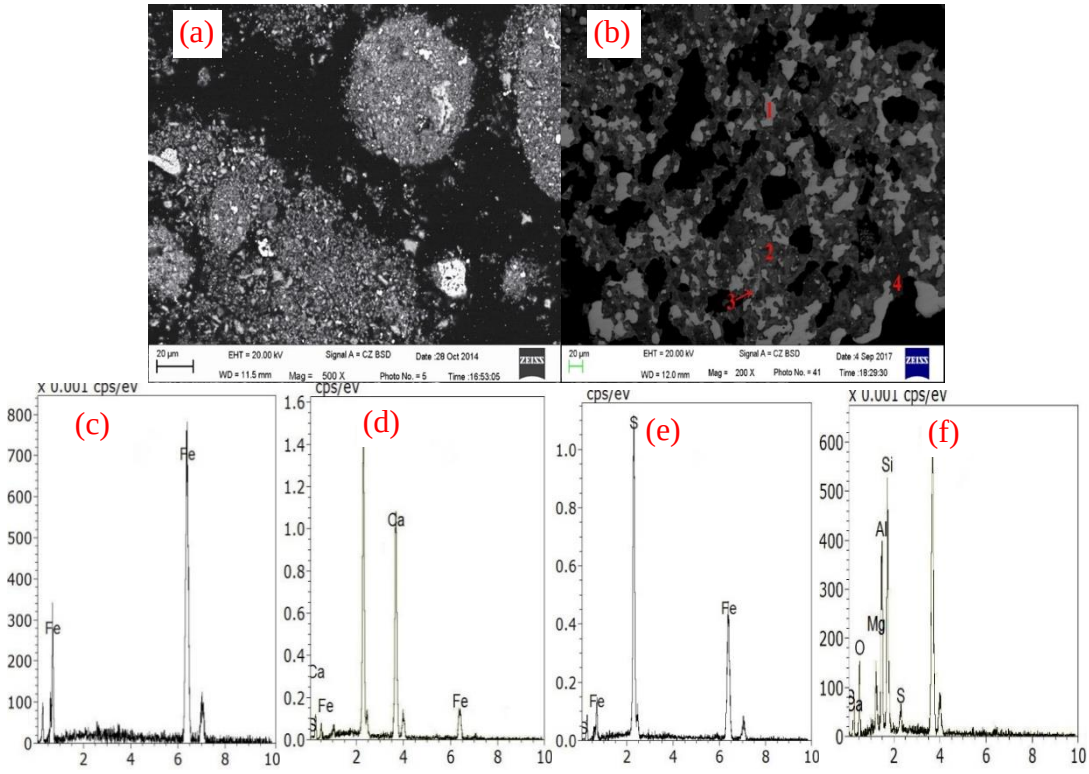

Fig. 8. SEM image of jarosite (a) and reduction product under optimum conditions (b), corresponding EDS at Point 1 (c); Point 2 (d); Point 3 (e); Point 4 (f)

The main elements and their enrichment area of the reduction product under optimum conditions were analyzed by surface scan, as shown in Fig. 9. The Fig. 9 showed that Fe, Si, Ca, S and Al were the main elements in the reduction product. Fe, Si, S, Ca and Al had different enrichment areas which also indicated metallic iron can be separated from other substances. The Cr, which was not found in XRF analysis of jarosite, was not an element of jarosite itself, it was contamination during the sample polishing process. There was no As element in the surface scan, which meant As was volatilized. Some elements such as Sb, Cd have not been found in the surface scan, which indicated the reduction product contained very small amounts of these elements.

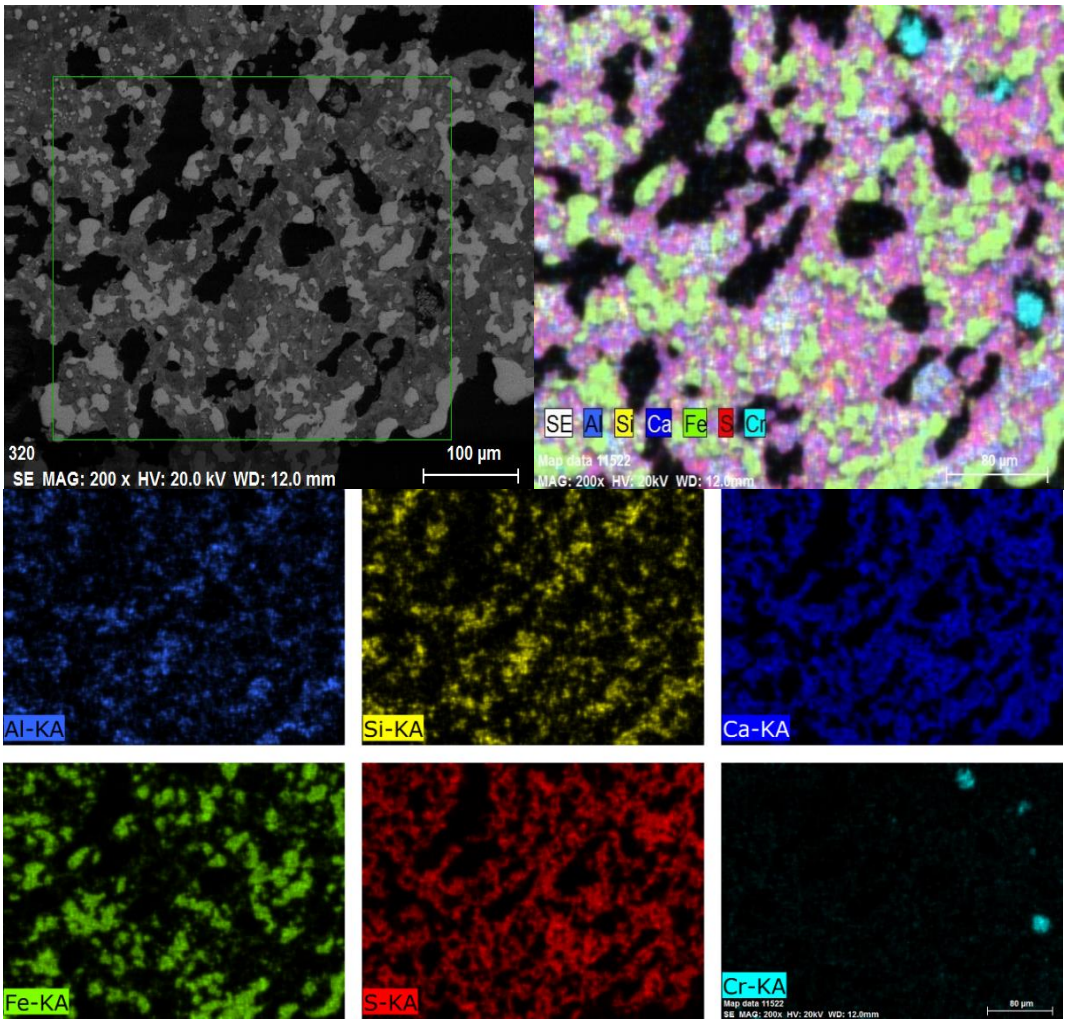

Fig. 9. Surface scan images of reduction product under optimum conditions

3.4 The recovery of iron

Under the conditions of the reduction product with grinding to 96.56% less than 37 µm and magnetic separation using the magnetic field strength of 24 kA/m, a concentrate was obtained with iron content of 90.59% and recovery of 50.87%. At this iron grade, the magnetic concentrate could be used as a raw material for electric furnace steelmaking, or powder metallurgy. However, some iron was lost to the magnetic tailings. The XRD of magnetic tailings was analyzed, and the results are shown in Fig. 10. Fig. 10 showed that the iron in the magnetic tailings existed mainly in the form of FeS, $Ca_2Fe_2O_5$ and a little metallic iron. In order to ensure that the sulfur content of the magnetic concentrate meets the requirement, the weakly magnetic FeS has to be discarded into the magnetic tailings which leads to low recovery of iron. According to Fig. 8 (d) and Fig. 10, some metallic iron is lost in the magnetic tailings. Besides, the non-magnetic $Ca_2Fe_2O_5$ existing in tailings also lead to the low recovery of iron.

Through direct reduction followed by magnetic separation, the distribution and content of heavy metals and precious metals in jarosite residue and its products were shown in Table 3. The Table 3 shows that almost all the Pb and Zn were volatilized into smoke dust, and the iron concentrate and tailings contained low content of lead and zinc. The precious metals Ga, Ge and Ag distributed in different products. 74.35% of Ga was volatilized into smoke dust. Nearly half of Ge was in the iron concentrate, the distribution rate and content were 55.94% and 109.0 g/Mg, respectively. The distribution rate and content of Ag in tailings were 69.92% and 115.0 g/Mg, which have high value for recovery and utilization.

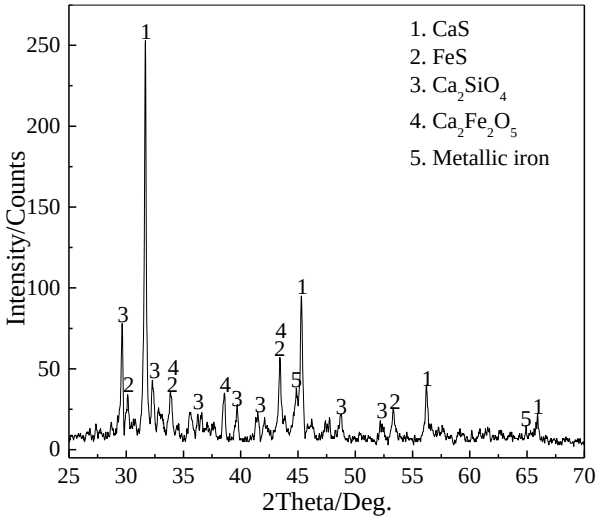

Fig. 10. XRD pattern of magnetic tailings

Table 3. The distribution and content of heavy metals and precious metals (wt-%)

Element	Content / wt-%			Distribution rate / wt-%		
	Jarosite	Iron concentrate	Tailings	Smoke dust	Iron concentrate	Tailings
Fe	26.76	90.57	23.26	0	50.87	49.13
Pb	3.01	0.04	0.14	96.97	0.21	2.82
Zn	6.95	0.01	0.009	99.89	0.03	0.08
Ga	56 g/Mg	53.9 g/Mg	9.6 g/Mg	74.35	15.37	10.28
Ge	31 g/Mg	109.0 g/Mg	12.4 g/Mg	20.00	55.94	24.06
Ag	98.4 g/Mg	100.0 g/Mg	115.0 g/Mg	13.86	16.22	69.92

4. Conclusions

Based on the present investigation, the following conclusions can be derived.

(1) Under the optimum reduction conditions of roasting at 1523 K for 60 min, the volatilization rates of lead, zinc and sulfur were 96.97%, 99.89% and 1.09% respectively and the iron metallization rate was 91.97%.

(2) A direct reduction iron with 90.59% iron can be obtained at a recovery rate of 50.87%. The weak magnetic FeS, non-magnetic $Ca_2Fe_2O_5$ and some metallic iron existing in CaS in the magnetic tailings lead to the low recovery of iron.

(3) The results show that the feasibility of the recovery of lead, zinc, iron from jarosite residues and simultaneous sulfur fixation by direct reduction and magnetic separation. This new method greatly reduces the harm of jarosite to the environment and provides the possibility of comprehensive utilization of hazardous jarosite residues.

References

ASOKAN, P., SAXENA, M., ASOLEKAR, S., 2010. *Recycling hazardous jarosite waste using coal combustion residues*.

Materials Characterization. 61, 1342-1355.

ASOKAN, P., SAXENA, M., ASOLEKAR, S.R., 2006. *Hazardous jarosite use in developing non-hazardous product for engineering application*. Journal of hazardous materials. 137, 1589-1599.

CALLA-CHOQUE, D., NAVA-ALONSO, F., FUENTES-ACEITUNO, J., 2016. *Acid decomposition and thiourea leaching of silver from hazardous jarosite residues: Effect of some cations on the stability of the thiourea system.* Journal of Hazardous Materials. 317, 440-448.

CHEN, Y., TANG, M., YANG, S., HE, J., TANG, C., YANG, J., LU, J., 2009. *Novel technique of decomposition of ammonium jarosite bearing indium in NaOH medium*. The Chinese Journal of Nonferrous Metals. 7, 028.

ERDEM, M., ÖZVERDI, A., 2011. *Environmental risk assessment and stabilization/solidification of zinc extraction residue: II. Stabilization/solidification.* Hydrometallurgy. 105, 270-276.

FROST, R.L., WILLS, R.-A., KLOPROGGE, J.T., MARTENS, W., 2006. *Thermal decomposition of ammonium jarosite* $(NH_4)Fe_3(SO_4)_2(OH)_6$. Journal of Thermal Analysis and Calorimetry. 84, 489-496.

GANG, Y., NING, P., LAN, Z., LIANG, Y.J., ZHOU, X.Y., BING, P., CHAI, L.Y., YANG, Z.H., 2015. *Selective reduction process of zinc ferrite and its application in treatment of zinc leaching residues.* Transactions of Nonferrous Metals Society of China. 25, 2744-2752.

GUO, D., HU, M., PU, C., XIAO, B., HU, Z., LIU, S., WANG, X., ZHU, X., 2015. *Kinetics and mechanisms of direct reduction of iron ore-biomass composite pellets with hydrogen gas.* International Journal of Hydrogen Energy. 40, 4733-4740.

HAN, H., SUN, W., HU, Y., JIA, B., TANG, H., 2014. *Anglesite and silver recovery from jarosite residues through roasting and sulfidization-flotation in zinc hydrometallurgy*. Journal of hazardous materials. 278, 49-54.

HU, H., DENG, Q., LI, C., XIE, Y., DONG, Z., ZHANG, W., 2014. *The recovery of Zn and Pb and the manufacture of lightweight bricks from zinc smelting slag and clay.* Journal of hazardous materials. 271, 220-227.

JU, S., ZHANG, Y., ZHANG, Y., XUE, P., WANG, Y., 2011. *Clean hydrometallurgical route to recover zinc, silver, lead, copper, cadmium and iron from hazardous jarosite residues produced during zinc hydrometallurgy.* Journal of hazardous materials. 192, 554-558.

KEROLLI-MUSTAFA, M., MANDIĆ, V., ĆURKOVIĆ, L., ŠIPUŠIĆ, J., 2016. *Investigation of thermal decomposition of jarosite tailing waste.* Journal of Thermal Analysis and Calorimetry. 123, 421-430.

LIU, W., YANG, J., XIAO, B., 2009. *Application of Bayer red mud for iron recovery and building material production from alumosilicate residues.* Journal of hazardous materials. 161, 474-478.

LIU, Z.G., SUN, T.C., WANG, X.P., GAO, E.X., 2015. *Generation process of FeS and its inhibition mechanism on iron mineral reduction in selective direct reduction of laterite nickel ore.* International Journal of Minerals, Metallurgy, and Materials. 22, 901-906.

MALENGA, E.N., MULABA-BAFUBIANDI, A., NHETA, W., 2015. *Alkaline leaching of nickel bearing ammonium jarosite precipitate using KOH, NaOH and* NH_4OH *in the presence of EDTA and* Na_2S. Hydrometallurgy. 155, 69-78.

MAWEJA, K., MUKONGO, T., MUTOMBO, I., 2009. *Cleaning of a copper matte smelting slag from a water-jacket furnace by direct reduction of heavy metals.* Journal of Hazardous Materials. 164, 856-862.

MONTANARO, L., BIANCHINI, N., RINCON, J.M., ROMERO, M., 2001. *Sintering behaviour of pressed red mud wastes from zinc hydrometallurgy.* Ceramics international. 27, 29-37.

ÖZVERDİ, A., ERDEM, M., 2010. *Environmental risk assessment and stabilization/solidification of zinc extraction residue: I. Environmental risk assessment.* Hydrometallurgy. 100, 103-109.

PAPPU, A., SAXENA, M., ASOLEKAR, S.R., 2006. *Jarosite characteristics and its utilisation potentials.* Science of the total environment. 359, 232-243.

PARK, J.W., AHN, J.C., SONG, H., PARK, K., SHIN, H., AHN, J.S., 2002. *Reduction characteristics of oily hot rolling mill sludge by direct reduced iron method.* Resources, conservation and recycling. 34, 129-140.

SUN, Y., HAN, Y., GAO, P., YU, J., 2015. *Size distribution behavior of metallic iron particles in coal-based reduction products of an oolitic iron ore.* Mineral Processing and Extractive Metallurgy Review. 36, 249-257.

YANG, H., JING, L., ZHANG, B., 2011. *Recovery of iron from vanadium tailings with coal-based direct reduction followed by magnetic separation.* Journal of hazardous materials. 185, 1405-1411.

YU, W., SUN, T., CUI, Q., XU, C., KOU, J., 2015. *Effect of Coal Type on the Reduction and Magnetic Separation of a High-phosphorus Oolitic Hematite Ore.* ISIJ International. 55, 536-543.